

Electronic and Magnetic Properties of Partially-Open Carbon Nanotubes

Bing Huang^{1,2}, Young-Woo Son³, Gunn Kim^{2*}, Wenhui Duan¹, and Jisoon Ihm^{2†}

¹*Department of Physics, Tsinghua University,
Beijing 100084, People's Republic of China*

²*FPRD and Department of Physics and Astronomy,
Seoul National University, Seoul 151-747, Republic of Korea*

³*Korea Institute for Advanced Study, Seoul 130-722, Republic of Korea*

(Dated: November 2, 2018)

Abstract

On the basis of the spin-polarized density functional theory calculations, we demonstrate that partially-open carbon nanotubes (CNTs) observed in recent experiments have rich electronic and magnetic properties which depend on the degree of the opening. A partially-open armchair CNT is converted from a metal to a semiconductor, and then to a spin-polarized semiconductor by increasing the length of the opening on the wall. Spin-polarized states become increasingly more stable than nonmagnetic states as the length of the opening is further increased. In addition, external electric fields or chemical modifications are usable to control the electronic and magnetic properties of the system. We show that half-metallicity may be achieved and the spin current may be controlled by external electric fields or by asymmetric functionalization of the edges of the opening. Our findings suggest that partially-open CNTs may offer unique opportunities for the future development of nanoscale electronics and spintronics.

* E-mail address: gunnkim@phya.snu.ac.kr

† E-mail address: jihm@snu.ac.kr

I. INTRODUCTION

Carbon nanotubes (CNTs) are quasi one-dimensional nanostructures with unique electrical properties that make them ideal candidates for applications in nanoelectronics^{1,2,3,4,5,6,7}. Because bare CNTs alone do not satisfy the requirements for actual applications, considerable experimental and theoretical efforts have been directed toward tailoring the electrical and mechanical properties of CNTs through various methods^{5,6,7,8,9,10,11}. Among them, chemical functionalization/doping and the application of external electric/magnetic fields are known as being practically viable approaches to tailoring the electrical properties of CNTs^{5,7,12,13,14,15}. In general, carbon-based systems are promising candidates for spin-based applications such as spin-qubits and spintronics^{11,12,16,17,18,19,20}; they are believed to have exceptionally long spin coherence times because of the absence of the nuclear spin in the carbon atom and very weak spin-orbit interactions. Therefore, in addition to their unique electrical properties, designing and modulating the spin injection and spin transport in CNTs have drawn heightened attention.

Recently, some methods have been proposed for lengthwise (*i. e.*, along the CNT axis) cutting to produce graphene or narrow graphene nanoribbons (GNRs)^{21,22,23,24,25}; these include etching with a plasma or an oxidizing agent to unzip the CNT^{21,22,23}. Moreover, the CNT sidewalls can be opened longitudinally by lithium atoms (or transition metal nanoparticles) intercalation and followed by exfoliation^{24,25}. It is interesting that the degree of stepwise opening is controllable by the amount of oxidizing agent or lithium atoms (or transition metal nanoparticles); partially-open CNTs have been observed in transmission electron microscopy or scanning electron microscopy images^{21,22,24,25}. There also exist a few theoretical studies on the unzipping mechanism of CNTs into GNRs²⁶ and the electronic transport in partially unzipped CNTs¹¹.

Armchair CNTs are one-dimensional metals with Dirac-like states crossing the Fermi level, and GNRs have edge states around the Fermi level which can induce magnetic ground states¹⁷. Since a partially-open CNT is composed of both a CNT and a curved GNR, it is expected to have more diverse properties and its electronic properties could be sensitive to the cutting width (*i.e.*, the circumferential length of cutting) as well as the cutting length. The edges at the opening may be chemically active for further chemical modifications as well.

In this article, we systematically investigate physical and chemical properties of partially-open armchair CNTs using spin-polarized density functional theory (DFT) calculations. Our results show that the electronic structures change from a metal to a semiconductor as the electron is backscattered at the opening (defective region). When the cutting length increases further, spin-polarization arises at the zigzag edges of the opening. The spin-polarized states become increasingly more stable than the nonmagnetic (NM) states following the increase in the length of cutting. We also demonstrate below that external electric fields and chemical functionalization are effective ways of controlling the electronic and magnetic properties of the partially-open CNTs; they produce still other interesting properties such as electrical switching and half-metallicity.

II. COMPUTATIONAL METHODS AND MODELS

In the present study, electronic structure calculations were performed using the Vienna *Ab initio* Simulation Package (VASP)²⁷ within the framework of the DFT. The projector augmented wave (PAW) potentials²⁸ and the generalized gradient approximation with the Perdew-Burk-Ernzerhof (PBE) functional²⁹ were used to describe the core electrons and the exchange-correlation energy, respectively. The cutoff energy for the plane wave basis set was set to 400 eV. Energies were converged to 10^{-5} eV, and the residual forces on all atoms were converged to below 0.02 eV/Å. The supercell for the (8, 8) CNTs of 2.5 nm in length was considered for typical calculations and the distances between two adjacent CNTs were maintained at least 10 Å to avoid the interactions between them. Three Monkhost-Pack special k -point meshes yielded ~ 1 meV per atom convergence of the total energy. The geometrical structures obtained from optimization processes were used to investigate the electronic and magnetic behaviors under static external electric fields (E_{ext}); our test calculations for $E_{ext} \leq 0.5$ V/Å on partially-open (8, 8) CNTs showed that the geometry relaxation from E_{ext} had a negligible effect. E_{ext} was implemented using a dipole layer in the vacuum, following widely-used Neugebauer and Scheffler's method³⁰.

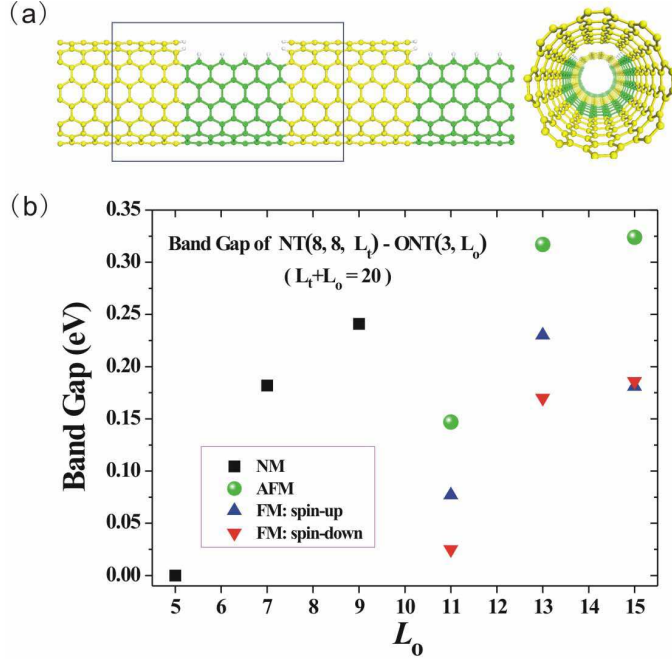


FIG. 1: (a) Structure of partially-open (m, n) CNTs (side view and the perspective view along the tube axis direction). Yellow and green balls represent carbon atoms on the perfect and the open CNT parts, respectively. The openings are passivated with hydrogen atoms, represented as small white balls. The rectangle marks one unit supercell in the tube axis direction of partially-open CNTs. The figure shows the structure of NT(8, 8, 11)-ONT(2, 9) representing a partially-open (8, 8) armchair CNT which has 11 (9) C-C dimer lines in the perfect CNT part (open part) along the tube axis direction, and the missing rows in the opening is 2. (b) The energy band gap as a function of the cutting length L_o (for $W = 3$). The band gaps of nonmagnetic (NM) materials are shown as black squares ($L_o \leq 9$). The band gaps of spin-polarized semiconductors with antiferromagnetic (AFM) or ferromagnetic (FM) states are shown as green dots and blue (red) triangles ($L_o \geq 11$), respectively.

III. RESULTS AND DISCUSSION

Geometries, Electronic and Magnetic Properties of Partially-Open CNTs. Before discussing our model structures, we first define a partially-open CNT, as shown in Figure 1a. A partially-open CNT has two parts: a perfect nanotube part (yellow color) and an opening (green color). This unit supercell is repeated periodically in the tube axis direction in the calculations. We represent the system as NT(m, n, L_t)-ONT(W, L_o) where m and n

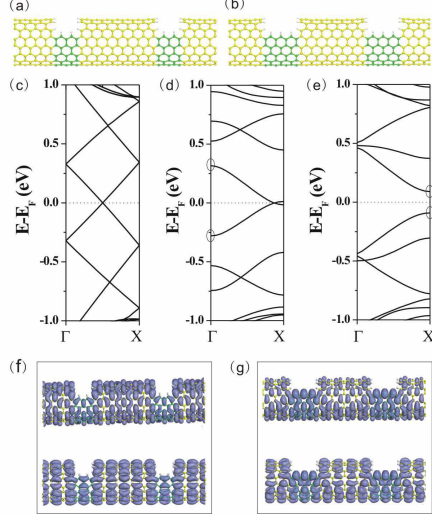


FIG. 2: Optimized structures (side view) of (a) NT(8, 8, 15)-ONT(3, 5) and (b) NT(8, 8, 13)-ONT(3, 7). (c) Electronic band structure of the perfect armchair (8, 8) CNT with a supercell size ten times the primitive unit cell. (d) and (e) are the band structures of NT(8, 8, 15)-ONT(3, 5) and NT(8, 8, 13)-ONT(3, 7), respectively. (f) Side view of the charge density on the top valence band (lower figure) and the bottom conduction band (upper figure) at Γ -point of the band structure in (d) (marked with circles). (g) Side view of the charge density on the top valence band (lower figure) and the bottom conduction band (upper figure) at X-point of the band structure in (e) (marked with circles). The Fermi level is set to zero.

correspond to the chiral vector of the CNT, L_t (L_o) is the length in the tube axis direction of the perfect (open) CNT in units of carbon columns, and W is the missing width in units of carbon rows for the opening. For example, the structure in Figure 1a can be designated as NT(8, 8, 11)-ONT(2, 9).

First, we will show the relation between electronic properties and the cutting length L_o with the cutting width W kept at 3. Figure 1b summarizes the results for NT(8, 8, L_t)-ONT(3, L_o) with different cutting lengths (L_o 's) while the total length of the supercell is kept unchanged ($L_t + L_o = 20$). When the cutting length was small, the overall structural relaxation was negligible. As the cutting length became longer, the middle part of the opening was widened to release the compressive stress and reduce the total energy. This agrees with experimental observations^{21,22,24,25}. (For optimized structures of NT(8, 8, L_t)-ONT(3, L_o), see Figure S1, Supporting Information.)

For $L_o \leq 5$, the system maintained its metallic character. The geometric and band

structures of NT(8, 8, 15)-ONT(3, 5) are shown as an example in Figures 2a and 2d. The band structure of the perfect (8, 8) CNT (the supercell was taken as ten times the primitive unit cell in order to match the Brillouin zone) is displayed in Figure 2c for comparison. Obviously, the energy degeneracies caused by the zone folding at the Brillouin zone boundary were lifted by the mirror symmetry breaking due to the existence of the opening (defect); however, no defect states were generated around the Fermi energy and the system was still metallic. Charge density analysis (Figure 2f) showed that the charge density around the Fermi energy was similar to that of a finite armchair CNT³¹ and some standing wave nodes occurred, which was due to the quantum confinement effects of the opening.

When the cutting length (L_o) was increased in a stepwise manner up to 9, ($5 < L_o \leq 9$), the system showed NM semiconducting behaviors. The band gap increased as L_o increased, as shown in Figure 1b. The geometric and band structures of NT(8, 8, 13)-ONT(3, 7) are shown in Figures 2b and 2e. Whereas the perfect (8, 8) CNT and NT(8, 8, 15)-ONT(3, 5) were metallic, NT(8, 8, 13)-ONT(3, 7) had a band gap of ~ 0.18 eV. Charge density analysis (Figure 2g) indicated that the gap opening was due to the breaking of the degeneracy of the original metallic states around the Fermi level (E_F).

For $L_o > 9$, the ground state changed from a NM state to a spin-polarized state. There were two stable spin-polarized states similar to that of zigzag graphene nanoribbons (ZGNRs)¹⁷, antiferromagnetic (AFM) and ferromagnetic (FM) state. The AFM configuration had the same spins lining up at each zigzag edge at the opening but with a relative spin orientation between two zigzag edges opposite to each other. On the other hand, the FM configuration had the same spins throughout. Both AFM and FM states were semiconducting while the NM state (which was unstable with respect to spin-polarized states) was metallic. The band gap of the spin-polarized states increased as the cutting length increased, as plotted in Figure 1b. The AFM state was the ground state for $L_o \geq 11$. For example, the energy of the AFM state was lower than the NM state by 0.050, 0.121, and 0.138 eV per unitcell for $L_o = 11, 13$, and 15, respectively. It was also lower in energy than the FM state by 0.03–0.05 eV per unitcell (see Table SI, Supporting Information). Since our calculations inevitably employed periodic supercells, a question arises whether our model can simulate a real system which does not have periodic openings. We contented ourselves with testing a longer unit cell where the interaction between two adjacent openings is significantly smaller than the above one ($L_t + L_o = 20$). Calculations performed for a longer unit cell

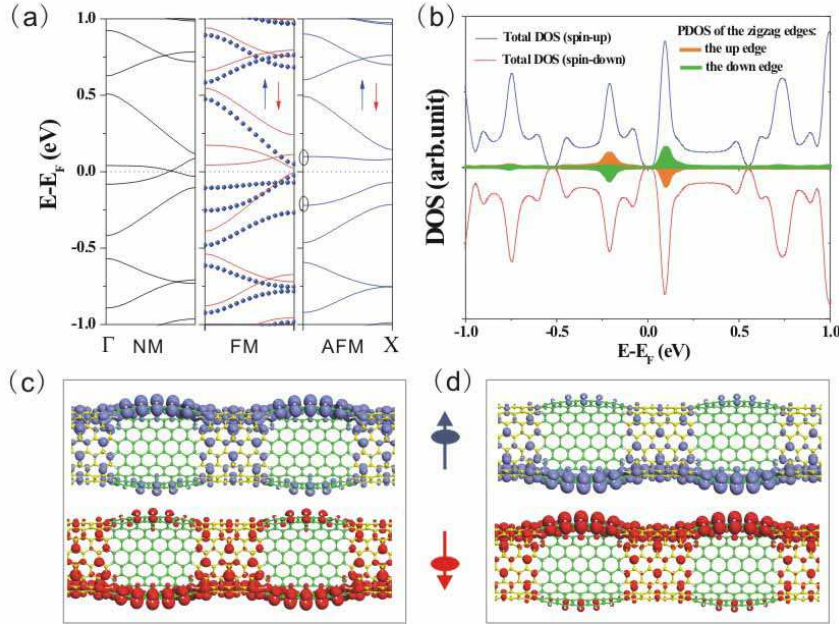


FIG. 3: Electronic structures and magnetic configurations of partially-open CNTs (a) Band structures of NT(8, 8, 9)-ONT(3, 11) for the NM, FM, and AFM states, respectively. Blue and red lines overlap and are indistinguishable in the AFM case. (b) Density of states (DOS) of NT(8, 8, 9)-ONT(3, 11) in the AFM ground state. The partial density of states (PDOS) of zigzag edges at the opening is also plotted as the green and orange-filled area inside the DOS curves. (c) The Γ -point charge density (top view) plots of two spin degenerate states on the top valence band of AFM state [lower circle in (a)]. (d) The Γ -point charge density (top view) plots of two spin degenerate states on the bottom conduction band of AFM state [upper circle in (a)]. In these figures, the blue and red colors represent the spin-up and spin-down states, respectively.

($L_t + L_o = 28$) produced essentially the same results as before (the conversion from a metal to an NM semiconductor to an AFM semiconductor), suggesting that the periodic supercell calculation should be a reasonable approximation in the present case.

Figure 3 shows the electronic properties of NT(8, 8, 9)-ONT(3, 11) as a prototype to demonstrate spin-polarized partially-open armchair CNTs. The NM state was metallic and unstable. Similar to perfect armchair CNTs, Dirac-like states were crossed at the E_F , as shown in the first panel of Figure 3a. Two Dirac-like states at the crossing point had different slopes, corresponding to different Fermi velocities. The second panel of Figure 3a displays a spin-split semiconducting FM state with band gaps of ~ 0.077 and ~ 0.025 eV for the

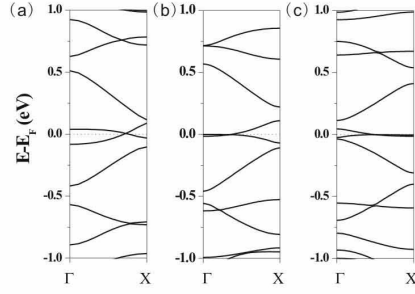


FIG. 4: The nonmagnetic band structures of (a) NT(8, 8, 9)-ONT(3, 11), (b) NT(8, 8, 7)-ONT(3, 13) and (c) NT(8, 8, 5)-ONT(3, 15).

spin-up and spin-down states, respectively. The magnetic moment of the FM state was close to $2 \mu_B$. The total energy calculation indicated that the FM state was not a ground state either; the AFM state was the ground state with a band gap of ~ 0.147 eV (or even larger gap for longer L_o). Spin distribution analysis (Figure S2, Supporting Information) showed that the spin polarization was mainly localized at the zigzag edges of the opening and that the spin moment at the center of the opening was largest ($\sim 0.23 \mu_B$ per atom). Small spin moments ($\sim 0.05 \mu_B$ per atom) were induced in the perfect CNT part. The states of the open zigzag edges were mainly located around the top valence band and the bottom conduction band; these are shown in the partial density of states (PDOS) (Figure 3b) and charge density plots (Figures 3c and 3d). The two spin states were located separately at opposite sides of the open zigzag edges, similar to those of ZGNRs¹⁷. Our previous work showed that the spin-polarization of ZGNRs could be understood in terms of the Stoner magnetism for sp electrons (instead of conventional d electrons) occupying a very narrow edge band (thus a huge density of states) to induce instability toward spin-band splitting³². Unlike ZGNRs, the NM state here only had Dirac-like bands crossing at the E_F . However, due to the opening, the DOS of the NM state near E_F increased (*i. e.*, the bands were flattened near E_F), as the cutting length L_o increased from 11 to 15, as shown in Figure 4. This presumably led to instability of the NM state and stabilized the spin-polarized state, analogous to ZGNRs.

We also show in Table I the relation between the electronic structure and the cutting width (W) for three different cutting lengths. For a short cutting length ($L_o = 5$), when W increased, a small band gap opened up because of the increased backscattering from

TABLE I: Energy band gap (in eV) as a function of the cutting width W for three different cutting length.

W	2	3	4
$L_o = 5$ (NM)	0	0	0.061
$L_o = 9$ (NM)	0.160	0.241	0.326
$L_o = 11$ (AFM)	0.112	0.147	0.195

TABLE II: Energy band gap (eV) as a function of the diameter of CNT for two different cuttings. ($L_t + L_o = 20$)

(W, L_o)	(6, 6) CNT	(8, 8) CNT	(10, 10) CNT
(3, 7) (NM)	0.337	0.182	0.099
(2, 11) (AFM)	0.117	0.112	0.099

the opening. For the middle cutting length ($L_o = 9$), the band gap increased significantly as W increased. For the spin-polarized one ($L_o = 11$), the band gap of the AFM ground state also became larger as W increased, while the stability of the AFM states (the energy difference between the AFM and NM states) did not change much (see Table SII, Supporting Information).

In order to investigate the curvature effect on electronic and magnetic properties of partially-open CNTs, we also calculated the electronic structures of (6, 6) and (10, 10) CNTs. Here, all the CNTs had the same supercell length along the axial direction. Similar to the (8, 8) CNT, the (6, 6) and (10, 10) CNTs showed the conversion from a metal to a semiconductor to a spin-polarized semiconductor by increasing the cutting length L_o . The relation between the band gap and the diameter of the CNT is listed in Table II. Two different cuttings corresponding to a nonmagnetic system ($W = 3, L_o = 7$) and a spin-polarized structure ($W = 2, L_o = 11$) were considered. For the nonmagnetic system ($W = 3, L_o = 7$), the band gap decreased remarkably from 0.337 eV to 0.099 eV, as the diameter of CNT increased. For the spin-polarized system ($W = 2, L_o = 11$), the AFM band gaps (for the ground state) decreased little (from 0.117 eV to 0.099 eV) as the diameter of CNT increased, demonstrating that the AFM band gap was insensitive to the diameter of the CNT.

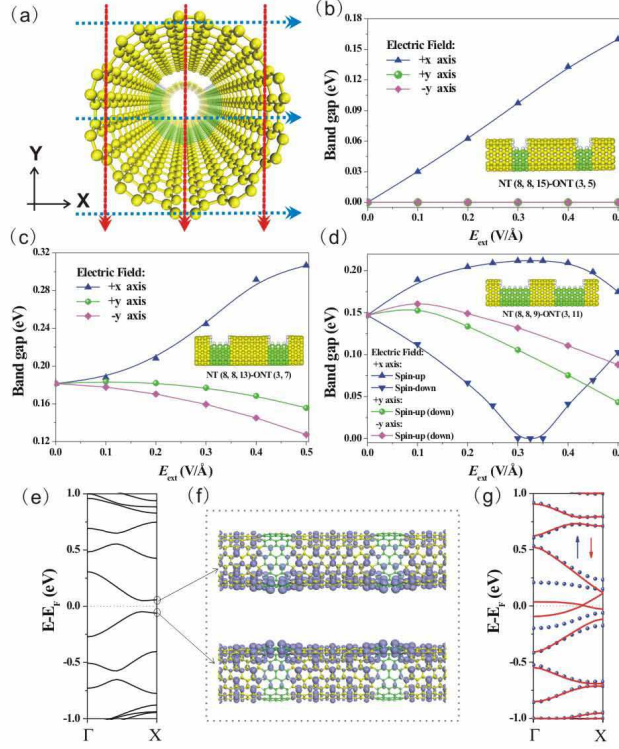


FIG. 5: Electronic properties of partially-open nanotubes with E_{ext} . (a) The model of partially-open armchair CNTs with E_{ext} . The band gaps as a function of E_{ext} are plotted for (b) NT(8, 8, 15)-ONT(3, 5), (c) NT(8, 8, 13)-ONT(3, 7), and (d) NT(8, 8, 9)-ONT(3, 11), respectively; the corresponding atomic structures (side view) are also shown as an inset in each case. (e) The band structure of NT(8, 8, 15)-ONT(3, 5) with $E_{ext} = 0.3 \text{ V/\AA}$ in the $+x$ direction. (f) Top view of the charge density on the top valence band (lower figure) and the bottom conduction band (upper figure) at the X-point of the band structure in (e) (marked with circles). (g) Spin-polarized band structure of NT(8, 8, 9)-ONT(3, 11) with $E_{ext} = 0.3 \text{ V/\AA}$ in the $+x$ direction.

Homogeneous External Electric Fields for Modulating Properties of Partially-Open CNTs. The response of CNTs to an external electric field (E_{ext}) is an interesting subject for future applications^{12,13}. The three directions of E_{ext} ($+x$, $+y$, $-y$), which were all perpendicular to the tube axis direction, z , were considered. It is noted that $+x$ is equivalent to $-x$ while $+y$ is not equivalent to $-y$ in the partially-open CNTs. Before the calculations of our system, some tests were done on the ZGNRs, using the E_{ext} method and the GGA approximation with the PBE functionals. Our tests showed that E_{ext} effect obtained from the GGA was significantly larger than that from the local density approximation (LDA); this was consistent

with previous observations^{33,34}. For example, the critical value of E_{ext} for half-metallicity in 16-ZGNR in our GGA calculations was ~ 0.55 V/Å, which was much larger than that from LDA calculations (~ 0.20 V/Å), and the difference agreed with previous works^{33,34}.

Figure 5 briefly summarizes the results of partially-open armchair CNTs affected by E_{ext} . Figure 5a shows the geometry and the directions of the E_{ext} , and Figures 5b-5d show the band gap behaviors for different cases. Our calculations on perfect armchair CNTs demonstrated that the band structure experienced little change in response to E_{ext} ; this was due to the strong screening behavior, which agreed well with previous results^{14,35,36}. For metallic NT(8, 8, 15)-ONT(3, 5) shown as the inset in Figure 5b, the system was still metallic when E_{ext} was in the $+y$ or $-y$ direction, as in the case of the perfect armchair CNT. However, when E_{ext} was applied in the $+x$ direction, the band gap opened up and drastically increased with the increase in the field strength. The band structure of NT(8, 8, 15)-ONT(3, 5) at 0.3 V/Å in the $+x$ direction is shown in Figure 5e. Compared with the unperturbed band structure (Figure 2d), the energy degeneracies were broken and a band gap appeared at the Fermi energy. The charge density of the top valence band and the bottom conduction band at the X-point are shown in Figure 5f. With E_{ext} in the $+x$ direction, the cylindrical symmetry of the charge density was broken, the top valence band around the X-point was localized mainly on the upper part of the tube, and the bottom conduction band around the X-point was localized mainly on the lower part of the tube. Therefore, the origin of the band gap opening was the Stark effect. For perfect armchair CNTs, extremely large E_{ext} (> 1.5 V/Å) was required for the band gap opening^{14,35,36}. NT(8, 8, 15)-ONT(3, 5) was now polarized with an induced dipole moment created by E_{ext} (Figure S3, Supporting Information). The charge density at the top valence band and the bottom conduction band changed little if E_{ext} was in the $+y$ or $-y$ direction. Thus, band structures showed little perturbation. In the case of semiconducting NT(8, 8, 13)-ONT(3, 7), shown as the inset of Figure 5c, the band gap increased to 0.30 eV when E_{ext} in the x direction reached 0.50 V/Å. The band gap decreased by only ~ 0.03 eV (~ 0.06 eV) at 0.50 V/Å in the $+y$ ($-y$) direction, and the redistributions of electrons at the top valence band and the bottom conduction band was not as pronounced as for E_{ext} in the $+x$ direction.

For NT(8, 8, 9)-ONT(3, 11) shown as an inset of Figure 5d, since the oppositely oriented spin states were located at opposite sides of the zigzag edge of the opening (Figure 3), the effect of E_{ext} on the spin states in the $+x$ direction on them should be opposite. This led to

the occupied spin-down states moving up and unoccupied spin-down states moving down, making the distance in energy closer, as shown in Figure 5d. The spin-up states behaved oppositely, enlarging the energy gap. This phenomenon was similar to the ZGNRs under transverse E_{ext} ¹⁷. The critical E_{ext} strength for half-metallic states (closing the band gap of the spin-down state) was around 0.3 V/Å. The corresponding band structure is shown in Figure 5g. Interestingly, the electronic structure of spin-down states around the Fermi energy was Dirac-like, unlike in ZGNRs. When E_{ext} was applied in the $+y$ or $-y$ direction, the band gaps of both spin states increased a little initially but decreased significantly under a stronger external field. Similar to the metallic open CNTs (Figure 5b) or the NM semiconductors (Figure 5c), the redistributions of the charge densities at the top valence band and the bottom conduction band was not pronounced for E_{ext} in the $+y$ or $-y$ direction. However, unlike in Figures 5b and 5c, E_{ext} in the $\pm y$ direction influenced the band gap more because the partially localized states around the E_F were substantially influenced by E_{ext} and thereby changing the band gap^{14,15,17,37}. Based on the behavior of spin states shown in Figures 5d and 5g, we propose that the partially-open CNT with E_{ext} may be used as a spin source to inject spin currents into the perfect CNT which is seamlessly connected to it.

We can explain the modification of band structures of partially-open CNTs in terms of the symmetry breaking as follows. For a perfect armchair CNT, the cylindrical symmetry and the mirror reflection symmetry are preserved. The π -bonding and π -antibonding (π^*) states are degenerate eigenstates crossing at the Fermi energy in this case. The wave functions in the π band do not have phase variation along the circumference of the tube whereas the signs of the wave functions in the π^* band alternate rapidly³⁸. However, the symmetry of our model structures becomes lower because of the openings. If the origin of the coordinate is set on the axis of the nanotube, our model structures retain the mirror reflection symmetry with respect to the $x = 0$ plane in the absence of the external fields. In contrast, they have no mirror reflection symmetry with respect to the $y = 0$ plane. When E_{ext} is applied in the $\pm x$ direction, the mirror reflection symmetry with respect to the $x = 0$ plane is broken as well. In Figure 5b, π and π^* states are no longer eigenstates in this situation and they become hybridized. Now the degeneracy is lifted and the band gap opens up rapidly as E_{ext} increases. For E_{ext} in the $\pm y$ direction, the mirror symmetry remains for the $x = 0$ plane and metallic partially-open CNTs maintain their metallic characters shown in Figure 5b. Since the screening effects of semiconducting partially-open CNTs are weak, however,

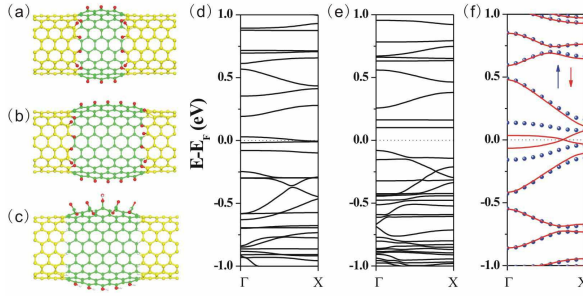


FIG. 6: Geometric and electronic structures of partially-open armchair CNTs with open edges modified with chemical groups: (a) NT(8, 8, 13)-ONT(3, 7) with O-termination; (b) NT(8, 8, 9)-ONT(3, 11) with O-termination; (c) NT(8, 8, 9)-ONT(3, 11) with two zigzag edges terminated with COOH and OH groups, respectively. (d), (e), and (f) correspond to electronic structures for (a), (b), and (c), respectively.

electronic structures of these CNTs do change a little bit even by E_{ext} in the $\pm y$ direction as shown in Figure 5c.

Chemical Functionalization for Modifying Properties of Partially-Open CNTs. Finally, we turn to chemical functionalization of CNTs. Chemical functionalization is an effective way to tailor the electronic and transport properties of CNTs^{5,7}. In an oxidative process, oxygen-containing functionalities such as carbonyl (C=O), carboxyl (COOH), and hydroxyl (OH) groups were observed to exist at the edge and on the surface of CNTs^{21,22,39,40,41}. As in the previous cases of the hydrogen passivation, the OH groups passivated the dangling sp^2 σ bonds at the open edges. Carbon π orbitals were affected by OH or H through the shift of the effective potential at the edge carbon atoms. When the edges in the opening were passivated with OH groups instead of H atoms, the overall shapes of the band structures did not change much (Figure S4, Supporting Information) but the band gap dramatically decreased. For example, the band gaps of NT(8, 8, 13)-ONT(3, 7) and NT(8, 8, 9)-ONT(3, 11) decreased by $\sim 50\%$ from 0.182 and 0.147 eV to 0.095 and 0.080 eV, respectively, shown in Figure S4 in Supporting Information. According to our calculations, the bond length between the O atom in the OH group and the edge carbon atom was ~ 1.36 Å.

Compared to H- or OH-termination, O-termination strongly modified the overall electronic structures of partially-open CNTs. In this case, each O atom was bonded to an edge carbon atom at the opening and its bond length was ~ 1.26 Å. In comparison, a carbon

dioxide (CO_2) molecule has a $\text{C}=\text{O}$ bond of $\sim 1.2 \text{ \AA}$. We chose O-terminated $\text{NT}(8, 8, 13)\text{-ONT}(3, 7)$ and $\text{NT}(8, 8, 9)\text{-ONT}(3, 11)$ to represent the spin-unpolarized and spin-polarized partially-open armchair CNTs, respectively. The optimized structures are depicted in Figures 6a and 6b. For $\text{NT}(8, 8, 13)\text{-ONT}(3,7)$, some localized states crossed at the Fermi energy, as shown in Figure 6d, and the charge density showed that edge O atoms and neighboring carbon atoms made major contributions to these states. The conductance of $\text{NT}(8, 8, 13)\text{-ONT}(3, 7)$ was greatly affected by those localized states. For $\text{NT}(8, 8, 9)\text{-ONT}(3, 11)$, the spin-polarization was suppressed and the ground state turned to the NM state, shown in Figure 6e, which was mainly due to the double bonds between C and O, destroying the edge states of the zigzag edges. Besides, some flat band states localized around the O atoms and the openings were produced below the bottom of the conduction band. Our results clearly showed that the oxygen should be avoided for spintronics applications of partially-open CNTs.

We also studied the electronic properties of partially-open CNTs with asymmetric edge functionalization as demonstrated for the ZGNRs⁴². We chose the COOH groups and the OH groups to terminate the two open zigzag edges of the spin-polarized $\text{NT}(8, 8, 9)\text{-ONT}(3, 11)$ structure, respectively, as shown in Figure 6c. The bond length between the carbon atom in the COOH group and the edge carbon atom at the opening was $\sim 1.47 \text{ \AA}$. The COOH group acted as an electron-acceptor whereas the OH group was effectively an electron donor. The asymmetric edge termination with COOH and OH groups resulted in a large potential difference between the two edges, and the effect was similar to applying electric fields in the x direction as studied before (Figures 5d and 5g). Figure 6f shows the spin splitting effect and the system became a half-metal as expected from the analogy to applied electric fields. Here, the half-metallicity was permanently established without external electric fields. Thus, we can conclude that the chemical modification is an efficient method of tailoring spin properties of our proposed system.

IV. SUMMARY

Using the spin-polarized density functional theory, we demonstrated that partially-open armchair CNTs had unusual electronic properties depending on the degree of opening. A partially-open armchair CNT was converted from a metal to a semiconductor to a spin-

polarized semiconductor by increasing the opening length. The spin-polarized states became more stable than nonmagnetic states with increase in the opening length. In addition, external electric fields and chemical functionalization were shown to be utilizable for controlling the electric and magnetic properties, as well as producing still other interesting properties such as electrical switching and half-metallicity.

Acknowledgments

The authors acknowledge the supports by the Core Competence Enhancement Program (2E21040) of KIST through the Hybrid Computational Science Laboratory, the SRC program (Center for Nanotubes and Nanostructured Composites) of MEST/KOSEF, the Korean Government MOEHRD, Basic Research Fund No. KRF-2006-341-C000015 (J.I.), the second BK21 program (G.K.), and KOSEF grant (Quantum Metamaterials research center, No. R11-2008-053-01002-0) funded by the MEST (Y.-W.S.). This work was also supported by the A3 Foresight Program of KOSEF-NSFC-JSPS, the Ministry of Science and Technology of China (Grant Nos. 2006CB605105, 2006CB0L0601), and the National Natural Science Foundation of China (W.D. and B.H.). The computations were performed through the support of KISTI in Korea.

Supporting Information Available:

This material is available free of charge via the Internet at <http://pubs.acs.org>.

-
- (1) Ijima, S., *Nature* **1991**, *354*, 56.
 - (2) Ijima, S.; Ichihashi, T. *Nature* **1993**, *363*, 603.
 - (3) Bethune, D. S.; Klang, C. H.; de Vries, M. S.; Gorman, G.; Savoy, R.; Vazquez, J.; Beyers, R. *Nature* **1993**, *363*, 605.
 - (4) Tans, S. J.; Verschueren, A. R. M.; Dekker, C. *Nature* **1998**, *393*, 49.
 - (5) Fischer, J. E. *Acc. Chem. Res.* **2002**, *25*, 1079.
 - (6) Javey, A.; Guo, J.; Wang, Q.; Lundstrom, M.; Dai, H. *Nature* **2003**, *424*, 654.
 - (7) Charlier, J. C.; Blase, X.; Roche, S. *Rev. Mod. Phys.* **2007**, *79*, 677.

- (8) Lee, S.; Kim, G.; Kim, H.; Choi, B.-Y.; Lee, J.; Jeong, B. W.; Ihm, J.; Kuk, Y.; Kahng, S.-J. *Phys. Rev. Lett.* **2005**, *95*, 166402.
- (9) Kim, S. H.; Choi, W. I.; Kim, G.; Song, Y. J.; Jeong, G.-H.; Hatakeyama, R.; Ihm, J.; Kuk, Y. *Phys. Rev. Lett.* **2007**, *99*, 256407.
- (10) Cha, M.; Jung, S.; Cha, M.-H.; Kim, G.; Ihm, J.; Lee, J. *Nano Lett.* **2009**, *9*, 1345.
- (11) Santos, H.; Chico, L.; Brey, L. *Phys. Rev. Lett.* **2009**, *103*, 086801.
- (12) Sahoo, S.; Kontos, T.; Furer, J.; Hoffmann, G.; Graber, M.; Cottet, A.; Schonenberger, C. *Nat. phys.* **2005**, *1*, 99.
- (13) Fedorov, G.; Lassagne, B.; Sagnes, M.; Raquet, B.; Broto, J.-M.; Triozon, F.; Roche, S.; Flahaut, E. *Phys. Rev. Lett.* **2005**, *94*, 066801.
- (14) Son, Y. -W.; Ihm, J.; Cohen, M. L.; Louie, S. G. *Phys. Rev. Lett.* **2005**, *95*, 216602.
- (15) Son, Y. -W.; Cohen, M. L.; Louie, S. G. *Nano Lett.* **2007**, *7*, 3518.
- (16) Petta, J. R.; Johnson, A. C.; Taylor, J. M.; Laird, E. A.; Yacoby, A.; Lukin, M. D.; Marcus, C. M.; Hanson, M. P.; Gossard, A. C. *Science* **2005**, *309*, 2180.
- (17) Son, Y. -W.; Cohen, M. L.; Louie, S. G. *Nature* **2006**, *444*, 347.
- (18) Nowack, K. C., Koppens, F. H. L., Nazarov, Yu. V.; Vandersypen, L. M. K. *Science* **2007**, *318*, 1430.
- (19) Awschalom, D. D.; Flatte, M. E. *Nat. phys.* **2007**, *3*, 153.
- (20) Tombros, N.; Jozsa, C.; Popinciuc, M.; Jonkman, H. T.; van Wees, B. J. *Nature* **2007**, *448*, 571.
- (21) Kosynkin, D. V.; Higginbotham, A. L.; Sinitskii, A.; Lomeda, J. R.; Dimiev, A.; Price, B. K. Tour, J. M. *Nature* **2009**, *458*, 872.
- (22) Zhang, Z.; Sun, Z.; Yao, J.; Kosynkin, D. V.; Tour, J. M. *J. AM. Chem. Soc.* **2009**, *131*, 13460.
- (23) Jiao, L.; Zhang, L.; Wang, X.; Diankov, G.; Dai, H. *Nature* **2009**, *458*, 877.
- (24) Cano-Márquez, A. G.; Rodríguez-Macias, F. J.; Campos-Delgado, J.; Espinosa-González, G.; Tristán-Lopez, F.; Ramírez-Gonzalez, D.; Cullen, D. A.; Smith, D. J.; Terrones, M.; Vega-Cantú, Y. *Nano Lett.* **2009**, *9*, 1527.
- (25) Elías, A. L.; Botello-Méndez, A. R.; Meneses-Rodríguez, D.; González, V. G.; Ramírez-González, D.; Ci, L.; Munoz-Sandoval, E.; Ajayan, P. M.; Terrones, H.; Terrones, M. *Nano Lett.* **2009**, doi: 10.1021/nl901631z.

- (26) Rangel, N. L.; Sotelo, J. C.; Seminario, J. M. *J. Chem. Phys.* **2009**, *131*, 031105.
- (27) Kresse, G.; Furthmüller, J. *Phys. Rev. B* **1996**, *54*, 11169.
- (28) Kresse, G.; Joubert, D. *Phys. Rev. B* **1999**, *59*, 1758.
- (29) Perdew, J. P.; Burke, K.; Ernzerhof, M. *Phys. Rev. Lett.* **1996**, *77*, 3865.
- (30) Neugebauer, J.; Scheffler, M. *Phys. Rev. B* **1992**, *46*, 16067.
- (31) Rubio, A.; Sánchez-Portal, D.; Emilio Artacho, E.; Ordejón, P.; and Soler, J. M.; *Phys. Rev. Lett.* **1999**, *82*, 3520.
- (32) Huang, B.; Liu, F.; Wu, J.; Gu, B. L.; Duan, W. H. *Phys. Rev. B* **2008**, *77*, 153411.
- (33) Hod, O.; Barone, V.; Peralta, J. E.; Scuseria, G. E. *Nano Lett.* **2007**, *7*, 2259.
- (34) Kan, E. J.; Li, Z. Y.; Yang, J. L.; Hou, J. G. *Appl. Phys. Lett.* **2007**, *91*, 243116.
- (35) Okeeffe, J.; Wei, C.; Cho, K. *Appl. Phys. Lett.* **2002**, *80*, 676.
- (36) Li, Y.; Rotkin, S. V.; Ravaioli, U. *Nano Lett.* **2003**, *3*, 183.
- (37) Tien, L. G.; Tsai, C. H.; Li, F. Y.; Lee, M. H. *Phys. Rev. B* **2005**, *72*, 245417.
- (38) Kim, G.; Lee, S. B.; Kim, T.-S.; Ihm, J. *Phys. Rev. B* **2005**, *71*, 205415.
- (39) Liu, J.; Rinzler, A. G.; Dai, H.; Hafner, J. H.; Bradley, R. K.; Boul, P. J.; Lu, A.; Iverson, T.; Shelimov, K.; Huffman, C. B.; Rodriguez-Macias, F.; Shon, Y. S.; Lee, T. R.; Colbert, D. T.; Smalley, R. E. *Science* **1998**, *280*, 1253.
- (40) Dujardin, E.; Ebbesen, T. W.; Krishnan, A.; Treacy, M. M. J. *Adv. Mater.* **1998**, *10*, 611.
- (41) Zhao, W.; Song, C.; Pehrsson, P. E. *J. Am. Chem. Soc.* **2002**, *124*, 12418.
- (42) Kan, E. J.; Li, Z. Y.; Yang, J. L.; Hou, J. G. *J. Am. Chem. Soc.* **2008**, *130*, 4224.